Physics of Fluids

RESEARCH ARTICLE | SEPTEMBER 05 2024

Hydrodynamic instability triggered during thin-film formation by interfacial polymerization

Adi M. Ben-Zvi ; Guy Z. Ramon

Physics of Fluids 36, 092104 (2024)
https://doi.org/10.1063/5.0214054

Physics of Fluids ARTICLE pubs.aip.org/aip/pof

Hydrodynamic instability triggered during thin-film formation by interfacial polymerization

Cite as: Phys. Fluids **36**, 092104 (2024); doi: 10.1063/5.0214054
Submitted: 17 April 2024 · Accepted: 6 August 2024 ·
Published Online: 5 September 2024

View Online Export Citation CrossMark

Adi M. Ben-Zvi[1,2] and Guy Z. Ramon[1,2,3,a)]

AFFILIATIONS

[1]Department of Civil and Environmental Engineering, Technion—Israel Institute of Technology, Haifa 32000, Israel
[2]Nanoscience and Nanotechnology Program, Technion—Israel Institute of Technology, Haifa 32000, Israel
[3]Wolfson Department of Chemical Engineering, Technion—Israel Institute of Technology, Haifa 32000, Israel

[a)]Author to whom correspondence should be addressed: ramong@technion.ac.il

ABSTRACT

An exothermic reaction at an immiscible liquid–liquid interface is at the core of several industrial processes and can trigger hydrodynamic instability. Here, we study interfacial polymerization, where a thin film is formed, whose morphology is known to be altered by synthesis conditions, impacting its industrial performance. Particle tracking microscopy is used to quantify fluid motion as a proxy for hydrodynamic instability intensity. Results indicate that, upon increasing polymerization-rate, particle motion transitions from Brownian to directed and is attributed to interfacially driven instabilities; concurrently, film morphology turns from smooth to crumpled. These results provide important insight for improved control over film fabrication.

Chemical reactions occurring at an immiscible liquid–liquid interface are of great importance in various industrial applications, including coatings, encapsulation, agrochemistry, and membrane fabrication for separation processes.[1–4] The chemical reaction is often exothermic and alters the physical properties of the fluids locally, which may result in flow, heat and mass transfer, and pattern forming instabilities.[5–9] The main mechanisms responsible for triggering and driving the instabilities are buoyancy, arising from alteration in fluid densities, and capillarity due to local differences in interfacial tension (IFT) (i.e., Marangoni flow).[2,8,10–13] Several experimental studies investigated the stability of interfaces, using a neutralization reaction as a model exothermic system; however, these have mostly been dominated by buoyancy.[2,6,14–16] Bratsun *et al.*[17] suggested that by eliminating gravitational effects, e.g., using a horizontal Hele–Shaw cell, Marangoni flow would possibly be observed. Subsequently, this configuration was realized using a neutralization reaction that forms surfactants at the interface.[18,19] Related theoretical studies considered the interfacial instability arising during the propagation of a polymerization front, under microgravity conditions,[20] as well as the stability of an immiscible liquid–liquid system with interfacial heat release,[8] revealing the potentially destabilizing effect of Marangoni stresses acting on the fluid at the interface generating a flow.

In the present case, we consider a different system and experimentally probe instabilities arising during a rapid, exothermic interfacial polymerization (IP) reaction, at an immiscible oil–water interface. This type of process is used extensively in industrial applications, notably micro-encapsulation and fabrication of separation membranes used in state-of-the-art water purification and desalination.[21–27] The primary outcome of IP is the formation of a thin film that serves as a semi-permeable barrier. Increasing evidence has pointed to the fact that the film morphology is strongly related to the formation dynamics (see Ref. 24 and references therein) and is intimately linked with the resultant film separation performance.[28–34] However, despite this important feature, the mechanisms connecting synthesis, morphology, and performance of IP-formed films are unresolved, while it has been suggested that film morphology is linked with possible instabilities triggered by the IP reaction.[23,24,31,35,36] In terms of the resultant film morphology, the assumption is that a smooth film is an outcome of a stable IP system, while a crumpled or multilayered film is indicative of the instability.[24]

In situ visualization methods are a powerful way to study the effect of synthesis conditions on stability during IP, but are challenging due to the high spatial and temporal resolutions required for tracking the rapid reaction and visualizing the very thin ($\sim$200 nm) resultant film.[23] Lately, studies have demonstrated real-time monitoring methods for IP, providing insights on reaction kinetics, transport, and film morphology; however, the effects on system's instability were not examined.[31,37–42] A recent study by Park *et al.*[36] visualized particle motion during IP using PIV (particle imaging velocimetry) of 1 μm fluorescent particles located in the aqueous phase within a horizontal Hele–Shaw microfluidic channel. Specifically, the effect of adding different surfactants to the aqueous solution was studied, revealing an increased velocity toward the interface upon increasing surfactant concentrations [below the critical micelle concentration (CMC)], as well as a more crumpled morphology of the formed film. They attributed this directed motion to a Marangoni instability occurring at the interface as a result of the IP reaction.[36] However, further fundamental understanding of the hydrodynamic instability in an IP system and its triggers is still required, specifically for connecting variable synthesis conditions, changed systematically, as well as providing strong evidence of the actual mechanism that drives the observed directed motion toward the interface.

Herein, we demonstrate how, in general, IP may manifest as a hydrodynamic instability, and how the main synthesis parameters—monomer concentrations and changes to solubility/IFT—conspire to dictate conditions that trigger the instability and its consequence in terms of the resultant film morphology. The basic premise of the experiments designed in the present study is that, by monitoring motion of particles in the fluid, during IP, a transition may be observed from trajectories typical of Brownian motion, expected in a quiescent fluid, to a directed motion indicative of a velocity field. This transition may manifest as hydrodynamic instability occurring in the system. The experimental system comprises a microfluidic Hele–Shaw horizontal cell that facilitates a pinned interface, established between two polydimethylsiloxane (PDMS)-molded cylinders (see Fig. 1, and supplementary material, for details). The aqueous phase, containing the monomer (here, we use m-phenylene diamine (MPD), which is typical of polyamide membranes) in specific concentrations (0.02%, 1%, or 2% w/v), along with 1-μm-diameter fluorescent polystyrene (PS) carboxylate-modified beads, orange (540/560) (Thermo Fisher) is injected into the right cylinder [Fig. 1(b)]. The creation of a water–air interface is monitored using the bright-field channel of the laser-scanning confocal microscope (TCS SP8, Leica). Next, a drop of the organic phase (oil), Isopar-G with, trimesoyl chloride (TMC, also typically used for polyamide membranes), at different concentrations (0.001%, 0.05%, 0.1% w/v), is injected using a syringe pump, through the hole on the right-hand side, while a second hole provides the exit path for the air and excess oil, if any. Live image acquisition commences a few seconds before the oil is injected, at ~40 fps and lasts for a total of 3000 frames. The series of images containing the fluorescent particles are then analyzed using the TrackMate plugin of FIJI software[43,44] (details in supplementary material), to obtain particle trajectories [Fig. 1(c)]. As previously mentioned, the characteristics of particle trajectories are used as a proxy for system stability. In a quiescent state, particles follow Brownian motion; in contrast, particles that exhibit directed motion may be evidence for the triggering of a hydrodynamic instability.[45] To provide a quantitative measure for the motion present, trajectory data were used to calculate the averaged linear velocity, defined as the net distance traversed by a particle [a straight line from the start to the end points, see Fig. 1(c)] divided by the tracking time, $\widehat{V}_l = \Delta l/\Delta t$ [Fig. 1(c) another parameter calculated is the motion linearity (LI), defined as the net distance divided by

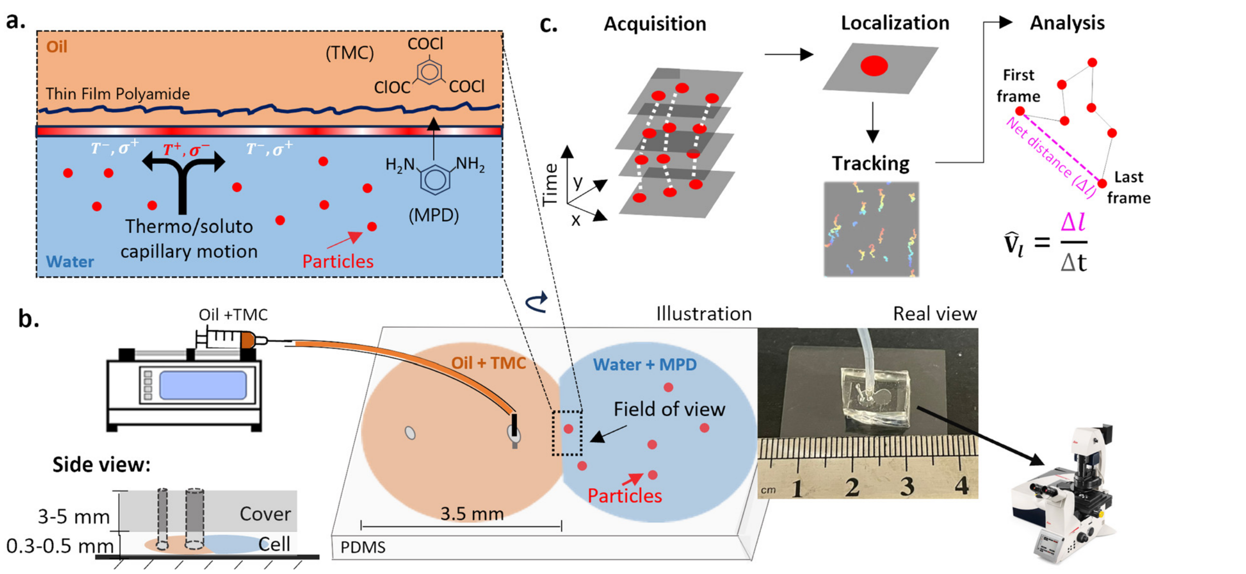

FIG. 1. Experimental methodology used to study the aqueous-phase dynamics during IP. (a) Schematic illustration of the IP system and its main features. Two immiscible phases are contacted, each containing a monomer, with preferential solubility toward the oil. Once contacted, the monomers react at the interface on the oil side, rapidly forming a thin-film (in the system studied, the monomers are TMC and MPD, typical monomers that form polyamide). Heat released during the reaction, as well as non-uniformities in monomer concentrations, may create local gradients in IFT (σ, red-white scale) along the interface, resulting in thermo-soluto-capillary motion and crumpling of the forming polyamide film. (b) Microfluidic IP system. Water containing MPD and 1 μm fluorescent particles is injected manually into the right side of a PDMS chip (which has a channel height of 300–500 μm, see side view), a horizontal Hele–Shaw cell. A confocal microscope is used to observe the aqueous side of the interface, while a syringe pump injects the oil (Isopar-G) containing TMC to the chip, and the second hole enables air release. (c) Data analysis. In the acquisition step, a series of fluorescent images are taken, imaging the particles. These images are then used to track the position of the particles, based on an intensity threshold, calculating trajectories and, consequently, the averaged linear velocity of the particles with respect to the interface.

the total distance traveled, see the supplementary material equation S1]. Finally, samples of IP-formed polyamide films were synthesized, under identical variations of the reaction conditions, using the so-called support-free IP (SFIP), following published protocols.[27,46] Briefly, the method relies on introducing the organic phase (containing TMC in Isopar-G) on top of the aqueous phase with MPD inside a bottom-closed Bu̇chner funnel, allowing the reaction to proceed for 1 min, after which it is terminated by pouring pure solvent (Isopar-G) on top and opening the bottom of the funnel, which enables collection of the polyamide film to the support membrane, see the supplementary material, Fig. S2. These samples were subsequently characterized by scanning electron microscopy (SEM) and atomic force microscopy (AFM) in order to provide morphological characteristics of the resultant film, under synthesis conditions corresponding with those employed during the microscopic visualization experiments, with the exception that the SFIP system does not eliminate gravitational effects. We note that the root mean square (RMS) roughness measured by the AFM is a limited measurement, because it does not account for increased morphological complexity beyond the deviations of the local surface height from the mean height. Hence, a multilayered morphology can have lower roughness than crumpled morphology;[24] therefore, we used the roughness as a qualitatively measurement.

In the set of experiments performed, conditions were varied systematically, to unravel the hypothesized change in system stability and resultant film morphology. Indeed, results demonstrate that increasing monomer concentrations from negligible (0.02% w/v MPD and 0.001% w/v TMC) to the "standard" concentration, C_0 (2% w/v MPD and 0.1% w/v TMC), generated motion within the aqueous phase, with a clear transition from Brownian to directed motion toward the interface [Fig. 2(b) (multimedia view) for 1% C_0 and for C_0], and Fig. S3(b), in supplementary material), an increased linear velocity, $\widehat{V}_l$, as well as linearity, LI [Figs. 2(c) and S4(a) in supplementary material], and a film morphology turning from smooth to nodular with increased roughness [Figs. 2(a), S5, and S6(a) in supplementary material]. The cause for this is presumably the increased initial MPD flux into the reaction zone, resulting in an increased polymerization rate[24,37,47] and hence more significant temperature and/or concentration gradients at the interface, driving a flow from low to high IFT (Marangoni) and a corresponding bulk flow of water to and from the interface. The gray region in Fig. 2(c) marks the $\widehat{V}_l$ calculated before the reaction, when the particles exhibit Brownian motion, as expected in a quiescent fluid.

To qualify the possible interfacially driven motion occurring in such a system, we estimated both solutal and thermal Marangoni numbers (see the supplementary material for details of this estimate). IFT values for different MPD concentrations were measured using a pendant drop method, and the IFT difference due to a temperature increase in 20^0 K (calculated by Wen *et al.*[48] in an analogous IP system) was estimated from a similar binary system (water + 2,3,4-trimethylpentane),[49] see equation S3, and Figs. S10–S12. The estimated solutal and thermal Marangoni numbers are $\sim 3.1 \times 10^5$ and $\sim 5.6 \times 10^3$, respectively, which manifest that the solutal variations are more prone to trigger the hydrodynamic instability. For a relatively similar reactive immiscible system, Bratsun and De wit estimated from their model a critical solutal Marangoni number of ~2000 and a thermal of $\sim 10^5$, from which convective Marangoni flow is observed in their system.[17] The coupling of solutal and thermal effects may magnify each other, and even a weak production of heat will have a strong effect on

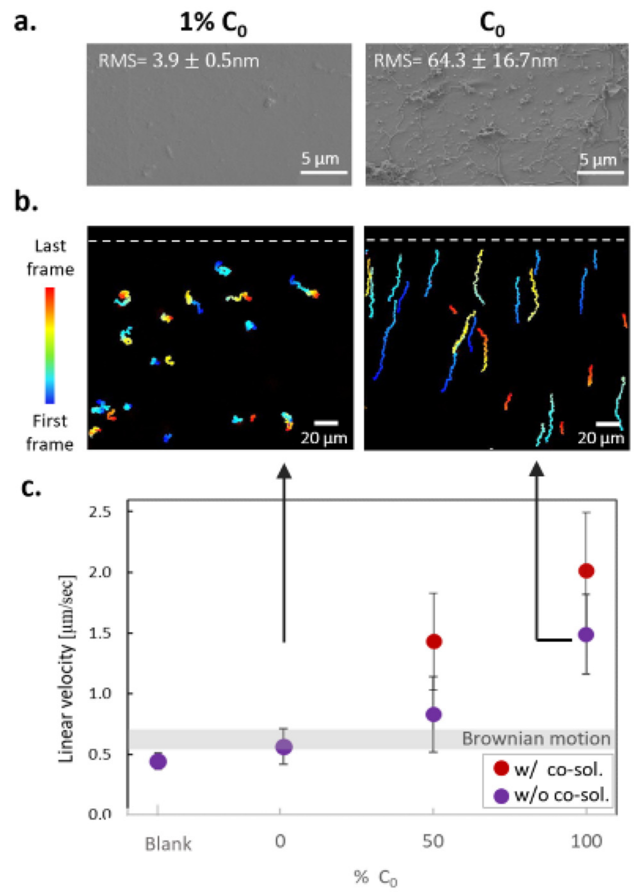

FIG. 2. Microscopic observation of particle motion and resultant film morphology for varying IP conditions. (a) Top-view SEM images of polyamide films fabricated via SFIP for 1% C_0, and C_0 (C_0 is the standard concentration, 2% w/v MPD and 0.1% w/v TMC) and the root mean square (RMS) surface roughness values measured by AFM. (b) Particle trajectories in the aqueous phase for IP at 1% C_0 and C_0. The track coloring changes with increasing frame number, from blue to red. The white dashed line marks the location of the interface. (c) Calculated linear particle velocity at increasing monomer concentrations (purple), and with added co-solvent, 2 wt. % ethyl acetate (red). The "blank" experiment is for standard MPD concentration with negligible IP reaction (0.001% w/v TMC). The gray region marks the linear motion calculated before injecting the organic phase, for presumably "Brownian" particles in this system. The linear velocity increases and the resultant film becomes rougher as monomer concentration is increased or a co-solvent is added. The error bars represent a 95% confidence interval. Multimedia available online.

the solutal instability.[17] Hence, we expect that our system would experience solutal capillary motion, which increases with increasing monomer concentrations and increased heat generation.

To further explore the reaction-induced motion, a co-solvent, ethyl acetate, was added to the organic solution at a fixed concentration (2% wt). The added co-solvent is expected to enhance the reaction rate due to the increased solubility of the aqueous monomer in the organic phase.[50,51] Furthermore, a co-solvent decreases the IFT, making the interface more deformable.[24] As seen in Fig. 2(c), the added co-solvent increases $\widehat{V}_l$ (red vs purple points), indicating a stronger instability, while also resulting in a rougher film morphology [see Fig. S6 supplementary material, film (a) vs (b) and (c) vs (d)]. When the co-solvent concentration is increased further, the motion increases as well (see the supplementary material, Fig. S7). As observed, by increasing the polymerization rate there is faster directed motion toward the interface [Figs. 2(b) and 2(c)], we assume that this motion is driven by an interfacial instability occurring at the interface due to the heat release and local monomer concentration gradients, as illustrated in Fig. 1(a). However, due to the experimental method, the full-convective motion could not be observed (we visualized the motion solely in the xy plane); therefore, phoretic motion of the colloidal PS particles may also generate the observed directed motion; here, we show why such motion is not observed here.

Local gradients in temperature, concentration, and pH that extend from the interface into the bulk solution[31,39] are evolved due to the exothermic nature of the IP reaction, the consumption of the alkaline MPD, and HCl release as a by-product, respectively appear in our system [see schematic illustration in Fig. 3(a)]. Such gradients may drive phoresis—thermal or diffusive—of the colloidal particles being tracked.[52–54] However, we believe that this is not what is driving the observed motion in our experiments, for the following reasons. First, thermophoresis, driven by temperature gradients, is expected to create particle motion down the gradient (particularly at temperatures above the ambient as expected in this case).[55,56] Shiundu *et al.* explicitly showed experimentally that PS particles migrate from hot to cold,[57] which is the exact opposite of the motion observed in our experiments. Diffusiophoresis, driven by solute concentration gradients, can be manifest during IP due to gradients in (H^+), and the aqueous monomer (MPD, in the case reported here). However, Shim *et al.*[58] showed experimentally that negatively charged PS particles (as used in our experiments) move toward the higher pH side—opposite to the direction reported here. Similarly, for gradients in MPD concentration (a non-electrolyte), diffusiophoresis are predicted to move up the concentration gradient,[59,60] for example, Paustrain *et al.* observed that carboxylated PS particles move up the concentration gradient of sucrose, a non-electrolyte.[61] However, it has also been shown that the direction of diffusiophoresis has a complex dependence on specific solute–particle interactions and in non-electrolyte as well as in polymer solutions, it can also be directed toward lower concentrations.[62,63]

To further rule out the possibility that the observed particle motion is due to diffusiophoresis, we performed a control experiment named as "blank" in Fig. 2(c), where the standard solution was used in the aqueous phase (particles and 2% w/v MPD), but at conditions generating a negligible IP reaction (0.001% w/v TMC in the organic phase, which helped stabilize the interface for visualization). The motion observed was "Brownian" with very low $\widehat{V}_l$ and LI, similar to the values observed for very low monomer concentrations [see Figs. 2(c), S3(a), and S4(a) blank and 1% C_0 in supplementary material]. These results conform with those obtained by Park *et al.*,[36] who also observed no directed motion when no reaction was present. Based on this collection of evidence, it is clear that the particle motion observed in our experiments cannot be attributed to diffusiophoresis.

To provide additional confirmation that the motion is driven by an interfacial instability, a final set of experiments was conducted, in which an anionic surfactant (sodium dodecyl-sulfate, SDS) was added, at different concentrations, to a system containing standard concentrations (C_0) of the monomers. In particular, concentrations were varied such that they ranged between 50% of the CMC to 10× the CMC, a concentration at which the interface is assumed to become immobilized by the surfactant—under such conditions, no interfacial motion would be possible.[64–72] In general, the presence of a negatively charged surfactant below its CMC can result in diffusiophoresis of like-charged colloidal particles down the SDS concentration gradient.[73–75] However, here we observed directed motion toward the interface below the CMC of SDS with increased $\widehat{V}_l$ and LI [see Fig. 3(b) and supplementary material Figs. S3(f) and S4(b) for the motion direction], which is up the SDS concentration gradient. Adding SDS increases the polymerization rate,[76] because it reduces the IFT[77,78] and the MPD

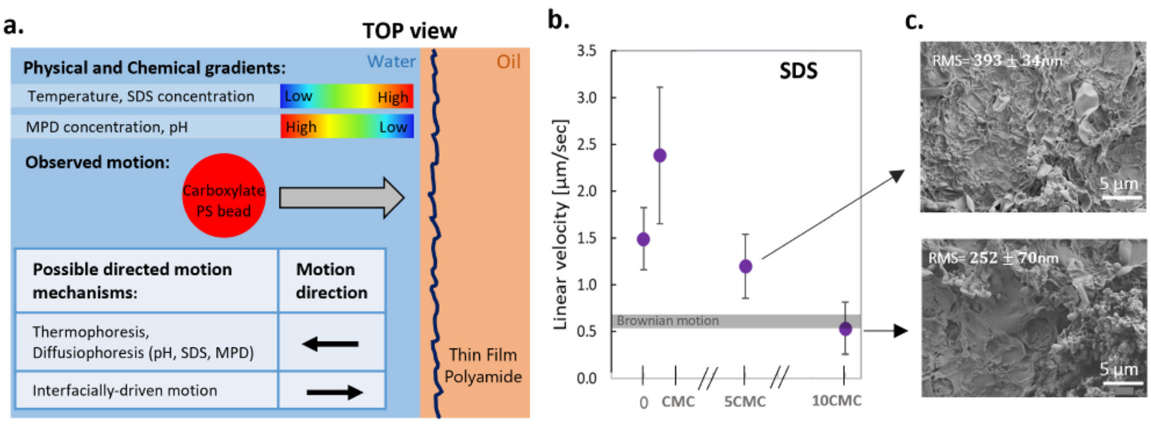

FIG. 3. Possible mechanisms for driving a directed motion and the hydrodynamic behavior when adding a surfactant as a possible explanation for the motion observations. (a) Mechanisms of possible directed motion as a result of physical and chemical gradients, which are evolved during the exothermic IP reaction at the immiscible aqueous-organic interface. The direction of the observed motion of the carboxylate-modified polystyrene (PS) beads toward the interface cannot be explained by thermophoresis or diffusiophoresis due to gradients in concentration or pH, which should result in motion in the opposite direction of the observed. However, a motion due to gradients tangential to the interface may cause the observed flow. (b) Linear velocity when adding SDS, to the aqueous phase in increasing concentrations, below and above the CMC when monomer concentrations are fixed, C_0. The gray region is the linear motion that was calculated before injecting the organic phase, when the particles followed Brownian motion. (c) SEM top-view images of polyamide membranes fabricated via SFIP with standard monomer concentrations: 2% w/v MPD and 0.1% w/v TMC, and SDS in the aqueous phase in concentration of 5XCMC (top), and 10XCMC (bottom). Root mean squared (RMS) surface roughness values measured by AFM with a 95% confidence interval.

partitioning to the organic phase is higher,[79] resulting also in rougher morphology [see Figs. S6(c) vs S6(e)]. However, above the CMC $\widehat{V}_l$ and LI first decrease and, eventually, at 10× the CMC, return to values typical of Brownian motion [Figs. 3(b) and S4(b), and for particle trajectories, see Figs. S3(g) and S3(h) in supplementary material]. It is important to note that, in the latter case, above the CMC of SDS, the IP reaction still takes place, as evidenced through the SEM images of the formed film [see Fig. 3(c)]. The crumpled morphology may be caused by foaming—bubbling of dissolved gases in the aqueous phase and/or vaporization of the organic phase due to increased temperatures in the reaction zone.[23,31,80,81] It may be exacerbated by the immobilization of the interface, which prevents convective heat transfer, as well as by the presence of surfactants that promotes bubble stability. Another possible explanation is that this crumpling is caused by attractive binding energy of SDS to MPD and to the polyamide film, resulting in SDS micelles incorporated into the film, causing its rupture and to irregular film morphology.[82] This leads to the conclusion that the observed motion toward the interface is driven by an interfacial instability, triggered by gradients in temperature and concentration during the IP reaction [as illustrated in Fig. 1(a)].

To conclude, this study provides evidence of instabilities that emerge during IP, the dependence on several governing synthesis parameters and, importantly, their contribution to the resultant film morphology. It is further demonstrated how hydrodynamic instability during interfacial reactions can be studied using a simple microfluidic system. This approach can enable further study of synthesis conditions and their impact on process performance, providing fundamental insight that can lead to improved design.

SUPPLEMENTARY MATERIAL

See the supplementary material for: (1) materials, (2) methods, (3) additional figures of SEM images, AFM roughness values, particle tracking trajectory maps, and (4) supplementary calculations.

ACKNOWLEDGMENTS

The research was supported by the Israel Science Foundation (Grant No. 3041/21). AB was supported, in part, by the Jewish National Fund (JNF)'s "climate" fellowship.

AUTHOR DECLARATIONS

Conflict of Interest

The authors have no conflicts to disclose.

Author Contributions

Adi M. Ben-Zvi: Conceptualization (equal); Formal analysis (lead); Investigation (lead); Methodology (equal); Project administration (lead); Visualization (equal); Writing – original draft (lead); Writing – review & editing (equal). **Guy Z. Ramon:** Conceptualization (equal); Funding acquisition (lead); Investigation (supporting); Methodology (supporting); Resources (lead); Supervision (lead); Visualization (equal); Writing – original draft (supporting); Writing – review & editing (equal).

DATA AVAILABILITY

The data that support the findings of this study are available within the article and its supplementary material.

REFERENCES

[1] A. Nepomnyashchy, I. Simanovskii, and J. Legros, *Interfacial Convection in Multilayer Systems* (Springer, 2006).

[2] K. Schwarzenberger, K. Eckert, and S. Odenbach, "Relaxation oscillations between Marangoni cells and double diffusive fingers in a reactive liquid-liquid system," Chem. Eng. Sci. **68**, 530–540 (2012).

[3] M. J. Raaijmakers and N. E. Benes, "Current trends in interfacial polymerization chemistry," Prog. Polym. Sci. **63**, 86–142 (2016).

[4] G. Ozkan, P. Franco, I. De Marco, J. Xiao, and E. Capanoglu, "A review of microencapsulation methods for food antioxidants: Principles, advantages, drawbacks and applications," Food Chem. **272**, 494–506 (2019).

[5] A. De Wit, K. Eckert, and S. Kalliadasis, "Introduction to the focus issue: Chemo-hydrodynamic patterns and instabilities," Chaos **22**, 037101 (2012).

[6] D. A. Bratsun, "On Rayleigh-Bénard mechanism of alignment of salt fingers in reactive immiscible two-layer systems," Microgravity Sci. Technol. **26**, 293–303 (2014).

[7] A. De Wit, "Chemo-hydrodynamic patterns in porous media," Phil. Trans. R. Soc. A **374**, 20150419 (2016).

[8] R. Patne, G. Z. Ramon, Y. Agnon, and A. Oron, "Dynamics of a two-layer flow with an interfacial heat source/sink: Viscosity stratification," J. Fluid Mech. **934**, A43 (2022).

[9] A. Mizev and A. Shmyrova, "Buoyancy-driven instabilities induced by a neutralization reaction in immiscible fluids," J. Phys.: Conf. Ser. **1809**, 012030 (2021).

[10] J. R. Pearson, "On convection cells induced by surface tension," J. Fluid Mech. **4**, 489–500 (1958).

[11] M. G. Velarde, "Drops, liquid layers and the Marangoni effect," Philos. Trans. R. Soc. London, Ser. A **356**, 829–844 (1998).

[12] A. De Wit, "Chemo-hydrodynamic patterns and instabilities," Annu. Rev. Fluid Mech. **52**, 531–555 (2020).

[13] D. Bratsun, A. Mizev, V. Utochkin, S. Nekrasov, and A. Shmyrova, "Nonlinear development of convective patterns driven by a neutralization reaction in immiscible two-layer systems," Philos. Trans. R. Soc. A **381**, 20220178 (2023).

[14] K. Eckert, M. Acker, and Y. Shi, "Chemical pattern formation driven by a neutralization reaction. I. Mechanism and basic features," Phys. Fluids **16**, 385–399 (2004).

[15] D. A. Bratsun, Y. Shi, K. Eckert, and A. D. Wit, "Control of chemo-hydrodynamic pattern formation by external localized cooling," Europhys. Lett. **69**, 746–752 (2005).

[16] Y. Shi and K. Eckert, "Acceleration of reaction fronts by hydrodynamic instabilities in immiscible systems," Chem. Eng. Sci. **61**, 5523–5533 (2006).

[17] D. A. Bratsun and A. De Wit, "On Marangoni convective patterns driven by an exothermic chemical reaction in two-layer systems," Phys. Fluids **16**, 1082–1096 (2004).

[18] S. Ying and K. Eckertb, "Orientation-dependent hydrodynamic instabilities from chemo-Marangoni cells to large scale interfacial deformations," Chin. J. Chem. Eng. **15**(5), 748–753 (2007).

[19] K. Eckert, M. Acker, R. Tadmouri, and V. Pimienta, "Chemo-Marangoni convection driven by an interfacial reaction: Pattern formation and kinetics," Chaos **22**, 037112 (2012).

[20] R. Texier-Picard, J. A. Pojman, and V. A. Volpert, "Effect of interfacial tension on propagating polymerization fronts," Chaos **10**, 224–230 (2000).

[21] Y. Song, J. B. Fan, and S. Wang, "Recent progress in interfacial polymerization," Mater. Chem. Front. **1**, 1028–1040 (2017).

[22] F. Zhang, J. b Fan, and S. Wang, "Interfacial polymerization: From chemistry to functional materials," Angew. Chem. Int. Ed. **59**, 21840–21856 (2020).

[23] V. Freger and G. Z. Ramon, "Polyamide desalination membranes: Formation, structure, and properties," Prog. Polym. Sci. **122**, 101451 (2021).

[24] I. Nulens, A. Ben Zvi, I. F. Vankelecom, and G. Z. Ramon, "Re-thinking polyamide thin film formation: How does interfacial destabilization dictate film morphology?," J. Membr. Sci. **656**, 120593 (2022).

[25] M. Busch and W. E. Mickols, "Reducing energy consumption in seawater desalination," Desalination **165**, 299–312 (2004).

[26] M. Elimelech and W. A. Phillip, "The future of seawater desalination: Energy, technology, and the environment," Science **333**, 712–717 (2011).

[27] Z. Jiang, S. Karan, and A. G. Livingston, "Water transport through ultrathin polyamide nanofilms used for reverse osmosis," Adv. Mater. **30**, 1–7 (2018).

[28]G. M. Geise, D. R. Paul, and B. D. Freeman, "Fundamental water and salt transport properties of polymeric materials," Prog. Polym. Sci. **39**, 1–42 (2014).
[29]L. Lin, R. Lopez, G. Z. Ramon, and O. Coronell, "Investigating the void structure of the polyamide active layers of thin- film composite membranes," J. Membr. Sci. **497**, 365–376 (2016).
[30]M. C. Wong, L. Lin, O. Coronell, E. M. Hoek, and G. Z. Ramon, "Impact of liquid-filled voids within the active layer on transport through thin-film composite membranes," J. Membr. Sci. **500**, 124–135 (2016).
[31]B. Ukrainsky and G. Z. Ramon, "Temperature measurement of the reaction zone during polyamide film formation by interfacial polymerization," J. Membr. Sci. **566**, 329–335 (2018).
[32]S. Mondal, I. M. Griffiths, and G. Z. Ramon, "Forefronts in structure–performance models of separation membranes," J. Membr. Sci. **588**, 117166 (2019).
[33]M. Stolov and V. Freger, "Membrane charge weakly affects ion transport in reverse osmosis," Environ. Sci. Technol. Lett. **7**, 440–445 (2020).
[34]S. P. Nunes, P. Z. Culfaz-Emecen, G. Z. Ramon, T. Visser, G. H. Koops, W. Jin, and M. Ulbricht, "Thinking the future of membranes: Perspectives for advanced and new membrane materials and manufacturing processes," J. Membr. Sci. **598**, 117761 (2020).
[35]S. Karan, Z. Jiang, and A. G. Livingston, "Sub-10 nm polyamide nanofilms with ultrafast solvent transport for molecular separation," Science **348**, 1347–1351 (2015).
[36]S.-J. Park, M.-S. Lee, M. E. Kilic, J. Ryu, H. Park, Y. I. Park, H. Kim, K.-R. Lee, and J.-H. Lee, "Autonomous interfacial assembly of polymer nanofilms via surfactant-regulated Marangoni instability," Nano Lett. **23**, 4822–4829 (2023).
[37]A. Nowbahar, V. Mansard, J. M. Mecca, M. Paul, T. Arrowood, and T. M. Squires, "Measuring interfacial polymerization kinetics using microfluidic interferometry," J. Am. Chem. Soc. **140**, 3173–3176 (2018).
[38]T. D. Matthews, H. Yan, D. G. Cahill, O. Coronell, and B. J. Mariñas, "Growth dynamics of interfacially polymerized polyamide layers by diffuse reflectance spectroscopy and Rutherford backscattering spectrometry," J. Membr. Sci. **429**, 71–80 (2013).
[39]S. Behera and A. K. Suresh, "Kinetics of interfacial polycondensation reactions – Development of a new method and its validation," Polymer **127**, 28–44 (2017).
[40]Y. Zhang, N. E. Benes, and R. G. Lammertink, "Visualization and characterization of interfacial polymerization layer formation," Lab Chip **15**, 575–580 (2015).
[41]J. H. Xin, B. B. Guo, C. Liu, C. Y. Zhu, H. Zhang, B. Z. Tang, and Z. K. Xu, "AIE-enabled in situ and real-time visualization of polymer growth during interfacial polymerization," Macromolecules **56**, 5415–5423 (2023).
[42]J. Mansouri, S. Huang, A. Agostino, R. P. Kuchel, G. Leslie, C. Y. Tang, and A. G. Fane, "Kinetics of support-free interfacial polymerization polyamide films by in-situ absorbance spectroscopy," Desalination **549**, 116349 (2023).
[43]D. Ershov, M. S. Phan, J. W. Pylvänäinen, S. U. Rigaud, L. Le Blanc, A. Charles-Orszag, J. R. Conway, R. F. Laine, N. H. Roy, D. Bonazzi, G. Duménil, G. Jacquemet, and J. Y. Tinevez, "TrackMate 7: Integrating state-of-the-art segmentation algorithms into tracking pipelines," Nat. Methods **19**, 829–832 (2022).
[44]J. Y. Tinevez, N. Perry, J. Schindelin, G. M. Hoopes, G. D. Reynolds, E. Laplantine, S. Y. Bednarek, S. L. Shorte, and K. W. Eliceiri, "TrackMate: An open and extensible platform for single-particle tracking," Methods **115**, 80–90 (2017).
[45]S. Sporer, C. Goll, and K. Mecke, "Motion by stopping: Rectifying Brownian motion of nonspherical particles," Phys. Rev. E **78**, 011917 (2008).
[46]S. J. Park, W. Choi, S. E. Nam, S. Hong, J. S. Lee, and J. H. Lee, "Fabrication of polyamide thin film composite reverse osmosis membranes via support-free interfacial polymerization," J. Membr. Sci. **526**, 52–59 (2017).
[47]V. Freger, "Kinetics of film formation by interfacial polycondensation," Langmuir **21**, 1884–1894 (2005).
[48]Y. Wen, R. Dai, X. Li, X. Zhang, X. Cao, Z. Wu, S. Lin, C. Y. Tang, and Z. Wang, "Metal-organic framework enables ultraselective polyamide membrane for desalination and water reuse," Sci. Adv. **8**, 4149 (2022).
[49]C. G. Aranda-Bravo, A. Romero-Martínez, A. Trejo, and J. Águila-Hernández, "Interfacial tension and density of water + branched hydrocarbon binary systems in the range 303–343 K," Ind. Eng. Chem. Res. **48**, 1476–1483 (2009).
[50]C. Kong, M. Kanezashi, T. Yamomoto, T. Shintani, and T. Tsuru, "Controlled synthesis of high performance polyamide membrane with thin dense layer for water desalination," J. Membr. Sci. **362**, 76–80 (2010).
[51]R. H. Hailemariam, J. S. Choi, M. M. Damtie, H. Rho, K. D. Park, J. Lee, and Y. C. Woo, "Enhancing performances of polyamide thin film composite membranes via co-solvent assisted interfacial polymerization," Desalination **524**, 115481 (2022).
[52]J. L. Anderson, "Transport mechanisms of biological colloids," Ann. New York Acad. Sci. **469**, 166–177 (1986).
[53]J. L. Anderson, "Colloid transport by interfacial forces," Annu. Rev. Fluid Mech. **21**, 61–99 (1989).
[54]A. S. Khair, "Diffusiophoresis of colloidal particles in neutral solute gradients at finite Péclet number," J. Fluid Mech. **731**, 64–94 (2013).
[55]S. Iacopini, R. Rusconi, and R. Piazza, "The "macromolecular tourist": Universal temperature dependence of thermal diffusion in aqueous colloidal suspensions," Eur. Phys. J. E **19**, 59–67 (2006).
[56]R. Piazza, "Thermophoresis: Moving particles with thermal gradients," Soft Matter **4**, 1740–1744 (2008).
[57]P. M. Shiundu, P. S. Williams, and J. C. Giddings, "Magnitude and direction of thermal diffusion of colloidal particles measured by thermal field-flow fractionation," J. Colloid Interface Sci. **266**, 366–376 (2003).
[58]S. Shim, J. K. Nunes, G. Chen, and H. A. Stone, "Diffusiophoresis in the presence of a pH gradient," Phys. Rev. Fluids **7**, 110513 (2022).
[59]J. L. Anderson and D. C. Prieve, "Diffusiophoresis: Migration of colloidal particles in gradients of solute concentration," Sep. Purif. Rev. **13**, 67–103 (1984).
[60]H. J. Keh, "Diffusiophoresis of charged particles and diffusioosmosis of electrolyte solutions," Curr. Opin. Colloid Interface Sci. **24**, 13–22 (2016).
[61]J. S. Paustian, C. D. Angulo, R. Nery-Azevedo, N. Shi, A. I. Abdel-Fattah, and T. M. Squires, "Direct measurements of colloidal solvophoresis under imposed solvent and solute gradients," Langmuir **31**, 4402–4410 (2015).
[62]P. O. Staffeld and J. A. Quinn, "Diffusion-induced banding of colloid particles via diffusiophoresis: 2. Non-electrolytes," J. Colloid Interface Sci. **130**, 88–100 (1989).
[63]R. P. Sear and P. B. Warren, "Diffusiophoresis in nonadsorbing polymer solutions: The Asakura-Oosawa model and stratification in drying films," Phys. Rev. E **96**, 062602 (2017).
[64]L. Ting, D. T. Wasan, and K. Miyano, "Longitudinal surface waves for the study of dynamic properties of surfactant systems: III. Liquid—liquid interface," J. Colloid Interface Sci. **107**, 345–354 (1985).
[65]N. Paul, M. Kraume, S. Schön, and R. von Klitzing, "Transport processes at single droplets in micellar liquid/liquid systems," AIChE J. **61**, 1092–1104 (2015).
[66]C. P. Baryiames and C. R. Baiz, "Slow oil, slow water: Long-range dynamic coupling across a liquid-liquid interface," J. Am. Chem. Soc. **142**, 8063–8067 (2020).
[67]T. Baier and S. Hardt, "Influence of insoluble surfactants on shear flow over a surface in Cassie state at large Péclet numbers," J. Fluid Mech. **907**, A3 (2021).
[68]Y. Touhami, D. Rana, V. Hornof, and G. H. Neale, "Effects of added surfactant on the dynamic interfacial tension behavior of acidic oil/alkaline systems," J. Colloid Interface Sci. **239**, 226–229 (2001).
[69]O. Manor, O. Lavrenteva, and A. Nir, "Effect of non-homogeneous surface viscosity on the Marangoni migration of a droplet in viscous fluid," J. Colloid Interface Sci. **321**, 142–153 (2008).
[70]O. Manor, I. U. Vakarelski, G. W. Stevens, F. Grieser, R. R. Dagastine, and D. Y. Chan, "Dynamic forces between bubbles and surfaces and hydrodynamic boundary conditions," Langmuir **24**, 11533–11543 (2008).
[71]N. F. Djabbarah and D. T. Wasan, "Relationship between surface viscosity and surface composition of adsorbed surfactant films," Ind. Eng. Chem. Fundam. **21**, 27–31 (1982).
[72]J. Chanda, S. Chakraborty, and S. Bandyopadhyay, "Monolayer of aerosol-OT surfactants adsorbed at the air/water interface: An atomistic computer simulation study," J. Phys. Chem. B **109**, 471–479 (2005).
[73]R. Nery-Azevedo, A. Banerjee, and T. M. Squires, "Diffusiophoresis in ionic surfactant gradients," Langmuir **33**, 9694–9702 (2017).
[74]P. B. Warren, S. Shin, and H. A. Stone, "Diffusiophoresis in ionic surfactants: Effect of micelle formation," Soft Matter **15**, 278–288 (2019).
[75]A. Banerjee, I. Williams, R. N. Azevedo, M. E. Helgeson, and T. M. Squires, "Soluto-inertial phenomena: Designing long-range, long-lasting, surface-specific

interactions in suspensions," Proc. Natl. Acad. Sci. U. S. A. **113**, 8612–8617 (2016).
[76] Y. Liang, Y. Zhu, C. Liu, K. R. Lee, W. S. Hung, Z. Wang, Y. Li, M. Elimelech, J. Jin, and S. Lin, "Polyamide nanofiltration membrane with highly uniform subnanometre pores for sub-1 Å precision separation," Nat. Commun. **11**, 1–9 (2020).
[77] B. Vafakish and L. D. Wilson, "A review on recent progress of glycan-based surfactant micelles as nanoreactor systems for chemical synthesis applications," Polysaccharides **2**, 168–186 (2021).
[78] R. J. Farn, *Chemistry and Technology of Surfactants* (Blackwell Publishing, 2006).
[79] Y. Li, T. H. Chen, C. Y. Yu, T. Wu, X. T. Zhao, J. F. Pan, and L. F. Liu, "Facile polyamide microstructure adjustment of the composite reverse osmosis membrane assisted by PF127/SDS mixed micelles for improving seawater desalination performance," Desalination **521**, 115395 (2022).
[80] X. H. Ma, Z. K. Yao, Z. Yang, H. Guo, Z. L. Xu, C. Y. Tang, and M. Elimelech, "Nanofoaming of polyamide desalination membranes to tune permeability and selectivity," Environ. Sci. Technol. Lett. **5**, 123–130 (2018).
[81] X. Song, B. Gan, Z. Yang, C. Y. Tang, and C. Gao, "Confined nanobubbles shape the surface roughness structures of thin film composite polyamide desalination membranes," J. Membr. Sci. **582**, 342–349 (2019).
[82] Q. Shen, Q. Song, Z. Mai, K. R. Lee, T. Yoshioka, K. Guan, R. R. Gonzales, and H. Matsuyama, "When self-assembly meets interfacial polymerization," Sci. Adv. **9**, eadf6122 (2023).